Valence orbitals of $W(CO)_6$ using electron momentum spectroscopy*

Shi Le-Lei(石砺磊), Liu Kun(刘 昆), Luo Zhi-Hong(罗志宏),
Ning Chuan-Gang(宁传刚)†, and Deng Jing-Kang(邓景康)†

Department of Physics and State Key Laboratory of Low-Dimensional Quantum Physics, Tsinghua University, Beijing 100084, *China*

(Received 4 March 2011; revised manuscript received 17 May 2011)

The binding energy spectra and the momentum distributions of the outer valence orbitals of $W(CO)_6$ have been studied by using electron momentum spectroscopy as well as non-relativistic, scalar relativistic and spin-orbital relativistic DFT-B3LYP calculations. The experimental momentum profiles of the outer valence orbitals obtained with the impact energies of 1200 eV and 2400 eV were compared with various theoretical calculation results. The relativistic calculations could provide better descriptions for the experimental momentum distributions than the non-relativistic ones. Moreover, a new ordering of orbitals $10t_{1u}$, $3t_{2g}$, and $7e_g$, i.e., $10t_{1u} < 3t_{2g} < 7e_g < 10a_{1g}$, is established in this work.

Keywords: $W(CO)_6$, electron momentum spectroscopy, relativistic effects

PACS: 34.80.Gs, 31.15.aj **DOI:** 10.1088/1674-1056/20/11/113403

1. Introduction

The theory of relativity and quantum mechanics are two of the most important scientific theories of the 20th century. While the latter was instantly applied to the chemistry research and produced quantum chemistry, the relativistic effects were considered to be "of no importance in the consideration of atomic and molecular structure and ordinary chemical reactions"[1] for a long time. Indeed it was not until the 1970s that the importance of the relativistic effects on atomic and molecular structure and in chemistry was fully appreciated.[2−7]

The relativistic effects in high-Z atoms and molecules containing high-Z atoms not only cause energy levels to shift and split, but also influence the electronic wave function. To understand the relativistic effects in chemistry, enormous progress haa been made on relativistic quantum chemical methods and calculations since the 1980s.[6,8−13] The relativistic methods can be roughly divided into the four-component, the two-component and the one-component relativistic methods.[14] The relativistic quantum chemical calculations have been an important theoretical implement for studying high-Z atoms and molecules containing high-Z atoms.[15,16]

In the experimental aspect, one of the most widely used methods to study the relativistic effects is photoelectron spectroscopy (PES),[17] which can measure the spin–orbital splitting energy and the branching ratio for spin–orbital splitting components as a function of the photon energy. Electron momentum spectroscopy (EMS),[18−20] also known as (e, 2e) spectroscopy, is another powerful tool to investigate the relativistic effects. It can measure both the orbital binding energy and the electron momentum distribution for each individual orbital.[21−23] The observed momentum distributions can be directly compared with the theoretical calculations under the assumptions of Born, binary encounter and plane-wave impulse (PWIA) approximations. This feature gives EMS the abilities to measure orbital electron densities and to evaluate basis sets and computational methods for the quantum chemistry. Although EMS has been used to investigate the relativistic effects for many years,[4,5,24−27] the applications were mainly limited to heavy atomic targets due to the complexity of the relativistic effects in a molecular target. Recently, a new method was developed, which can combine relativistic quantum chemistry theories with EMS

*Project supported by the National Natural Science Foundation of China (Grant Nos. 11074144, 10874097, and 10704046) and the Specialized Research Fund for the Doctoral Program of Higher Education, China (Grant No. 20070003146).

†Corresponding author. E-mail: ningcg@tsinghua.edu.cn; djk-dmp@tsinghua.edu.cn

© 2011 Chinese Physical Society and IOP Publishing Ltd

to study valence-electron structures of molecules.[28] With this method, molecules containing high-Z atoms could be studied using the EMS method.

The volatile transition metal carbonyls, tungsten hexacarbonyl ($W(CO)_6$), well-known as a precursor in the organometallic chemistry and as a model for the bond between CO and metal surfaces,[29] is an ideal molecular target for the gas phase EMS study on the relativistic effects in a molecule containing a high-Z atom. The previous EMS investigation of $W(CO)_6$ was performed together with $Cr(CO)_6$ and $Mo(CO)_6$ by Rolke *et al.*[30] with an impact energy of 1200 eV. They reported only the highest occupied molecular orbitals (HOMO) t_{2g}. A discernable discrepancy at the low momentum region was found between the experimental momentum profiles and the calculations using non-relativistic methods. Rolke *et al.* ascribed the discrepancy to the distorted wave effects. However, our recent work showed that the discrepancy was mainly due to the vibrational effects.[31]

In the present work, we report the momentum distributions associated to all the outer valence orbitals of $W(CO)_6$ except the HOMO with the impact energies of 1200 eV and 2400 eV with a higher resolution and a higher statistical accuracy. The influence of the relativistic effects is carefully considered to account for the high-Z W atom ($Z = 74$) in the $W(CO)_6$ molecule. The experimental momentum profiles are compared with the theoretical ones derived from the non-relativistic (NR), the scalar relativistic (SR) and the spin–orbital relativistic (SO) calculations using our new method.[28] The orbitals in the binding energy region from 14.5 eV to 17 eV assigned in the previous PES[32] work are reassigned based on the electron momentum distribution analysis. The results show that the relativistic method can provide a better description to the experiments than the non-relativistic one.

2. Experimental and theoretical methods

In a symmetric non-coplanar (e, 2e) experiment, the target molecules are ionized by an electron beam with high enough energy ($\sim$ keV) and the two outgoing electrons have almost equal kinetic energies and equal polar angles θ ($\theta_1 = \theta_2 = 45°$) respect to the incoming electron beam. The momentum of the electron prior to being knocked out can be determined through the out-of-plane azimuthal angle ϕ between the two outgoing electrons using equation

$$p = \left[(2p_1 \cos\theta - p_0)^2 + 4p_1^2 \sin^2\theta \sin^2\left(\frac{\phi}{2}\right)\right]^{1/2}, \quad (1)$$

where p_0 is the momentum of the incident electron and p_1 ($p_1 = p_2$) is the momentum of one of the two outgoing electrons. The plane wave impulse approximation is usually used to describe the collision under the conditions of high impact energy and high momentum transfer. Under the PWIA, the EMS differential cross section for randomly oriented gas-phase molecules is given by[18]

$$\sigma_{\mathrm{EMS}} \propto \int \frac{\mathrm{d}\Omega}{4\pi} \left| \left\langle \mathrm{e}^{-\mathrm{i}pr} \Psi_{\mathrm{f}}^{N-1} | \Psi_{\mathrm{i}}^{N} \right\rangle \right|^2, \quad (2)$$

where $\mathrm{e}^{-\mathrm{i}pr}$ is the plane wave function for the electrons, $\left|\Psi_{\mathrm{f}}^{N-1}\right\rangle$ and $\left|\Psi_{\mathrm{i}}^{N}\right\rangle$ are the total electronic wave functions for the final ion and the initial target molecule, respectively. The $\int \mathrm{d}\Omega$ indicates the spherical average, which accounts for the random orientations of the gas phase targets. Using the target Kohn–Sham approximation (TKSA) in the framework of the density functional theory (DFT),[33] equation (2) can be reduced to

$$\sigma_{\mathrm{EMS}} \propto \int \mathrm{d}\Omega \left|\psi_j^{\mathrm{KS}}(p)\right|^2, \quad (3)$$

where $\psi_j^{\mathrm{KS}}(p)$ is the momentum space Kohn–Sham orbital for the j-th electron. According to Eq. (3), EMS is able to image the electron density of an individual orbital selected according to the binding energy.

The details of our high resolution EMS spectrometer have been previously reported.[34,35] In short, our spectrometer takes the symmetric non-coplanar geometry. A double toroidal energy analyzer and position sensitive detectors are used to analyze the electron energy and the electron angles. An electron gun equipped with an oxide cathode is used, which works at much lower temperature than the generic filament cathodes. Since the oxide cathode is easily deactivated in an atmosphere of active gas, an additional vacuum chamber is specially designed for mounting the electron gun. The chamber, which has a hole of 2 mm in diameter for electron beam passing through, is evacuated to the base pressure of 10^{-6} Pa by using a molecular turbo pump. The energy resolution highly depends on the emitting current of the cathode due to the space charge effects. In the present work, an energy resolution ΔE of 0.68 eV (full width at half maximum (FWHM)] is obtained by controlling the emitting current.

The Amsterdam density functional (ADF) 2008 program[12,36,37] can perform relativistic and non-relativistic DFT calculations for atoms and molecules. The relativistic calculations include the scalar relativistic and the spin–orbital relativistic methods. The latter is one kind of two-component relativistic method, which can provide the spin–orbital splitting components. The scalar and the spin–orbital relativistic methods are incorporated via the zero order regular approximation (ZORA).[38] By means of the ADF, all calculations in the present work are performed using the standard hybrid Becke 3-Parameter Lee Yang and Parr (B3LYP) functional.[39] The NR calculations use the triple-zeta with one polarization (TZP) function basis sets with a frozen core shell up to the 4d level, while the relativistic calculations including the SR and the SO calculations use the ZORA/triple-zeta with two polarization (TZ2P) function basis sets without a frozen core. The optimized geometry of $W(CO)_6$ calculated by Ehlers and Frenking[40] is used for all the calculations, where the W–C bond length is $R_{W-C} = 2.0597$ Å and the C–O bond length is $R_{C-O} = 1.1655$ Å. The electronic wave function in the ADF program is constructed using the fragmental molecular orbital[12] and the double group representation[41,42] with the Slater type basis sets. The theoretical momentum distributions are generated using our NEMS[43] program. The molecular orbital generated using the spin–orbital relativistic ADF calculation has the form

$$\Psi(r) = \Psi_\alpha(r)\alpha + \Psi_\beta(r)\beta, \tag{4}$$

where α and β are the spin variables, $\Psi_\alpha(r)$ and $\Psi_\beta(r)$ are the space wave function components for spins α and β, respectively. The momentum distribution $|\Psi(p)|^2$ for the two-component molecular orbitals is obtained by

$$|\Psi(p)|^2 = |\Psi_\alpha(p)|^2 + |\Psi_\beta(p)|^2, \tag{5}$$

where $|\Psi_\alpha(p)|^2$ and $|\Psi_\beta(p)|^2$ are the momentum distributions for α and β spin components, respectively.

The $W(CO)_6$ sample is obtained commercially and is of 99.0% stated purity. The sample is solid and can sublime at room temperature. Since the volatility is not sufficient, we put the sample directly inside the spectrometer with a sample probe placed near the collision region. A heater with variable power, typically 0.4 W, is employed to control the density of the gaseous molecules. The measurement proceeds without further purifications. No impurity of the sample is evident in the binding-energy spectra.

3. Results and discussion

The tungsten hexacarbonyl ($W(CO)_6$) molecule contains 158 electrons and has an O_h symmetry point group. According to the scalar relativistic B3LYP/TZ2P calculation, the ground state electronic configuration can be written as

$$(\text{core})^{78}\underbrace{(7t_{1u})^6(1t_{2u})^6(1a_{2u})^2(8a_{1g})^2(8t_{1u})^6(5e_g)^4}_{\text{inner valence}}$$
$$\underbrace{(9a_{1g})^2(6e_g)^4(9t_{1u})^6(10a_{1g})^2(7e_g)^4(3t_{2g})^6(10t_{1u})^6(2t_{2u})^6(1t_{1g})^6(11t_{1u})^6(4t_{2g})^6}_{\text{outer valence}}.$$

The valence shell contains 17 molecular orbitals and can be divided into two sets: 6 inner valence and 11 outer valence orbitals. In the spin–orbital relativistic ADF calculations, each degenerate molecular orbital splits into two spin–orbital components.

3.1. Binding energy spectra

The ionization potentials measured by the PES[32] and the present EMS, as well as the NR, the SR and the SO orbital energies obtained in this work for the outer valence orbitals, are shown in Table 1. In the previous PES work,[32] $W(CO)_6$ showed many broad overlapping bands. The authors did not assign a peak for the $10a_{1g}$ orbital. They tentatively assigned the peaks between 14.5 eV and 17 eV to molecular orbitals with the ordering of $7e_g < 10t_{1u} < 3t_{2g} < 10a_{1g}$. However, our calculations with the NR and the SR methods give the ordering of $10t_{1u} < 3t_{2g} < 7e_g < 10a_{1g}$, which is also supported by our experimental electron momentum distributions. We will further discuss it in Section 3.3.

Table 1. Outer valence ionization potentials (IPs) for $W(CO)_6$ molecule in unit of eV.

Orbital No.	Orbital	Experimental		NR[d)]	SR[d)]	SO	
		EMS	PES[a)]			orbital	IPs[d)]
11	$4t_{2g}$	8.6	8.56	7.35	7.29	$4e_{5/2g}$	7.14
						$12u_{3/2g}$	7.36
10	$11t_{1u}$	13.4	13.27	11.45	11.83	$13u_{3/2u}$	11.69
						$11e_{1/2u}$	12.10
9	$1t_{1g}$		14.20	12.62	12.76	$11u_{3/2g}$	12.76
						$11e_{1/2g}$	12.77
8	$2t_{2u}$	14.3	14.42	12.76	12.91	$3e_{5/2u}$	12.90
						$12u_{3/2u}$	12.91
7	$10t_{1u}$		14.88[b)]	12.97	13.17	$11u_{3/2u}$	13.13
						$10e_{1/2u}$	13.27
6	$3t_{2g}$	15.0	15.2[b)]	13.22	13.35	$3e_{5/2g}$	13.34
						$10u_{3/2g}$	13.36
5	$7e_g$	15.7	15.54[b)]	13.49	13.52	$9u_{3/2g}$	13.52
4	$10a_{1g}$		–[c)]	13.71	14.27	$10e_{1/2g}$	14.27
3	$9t_{1u}$	17.9	17.84	15.83	16.00	$10u_{3/2u}$	15.97
						$9e_{1/2u}$	16.08
2	$6e_g$			16.14	16.24	$8u_{3/2g}$	16.25
1	$9a_{1g}$	20.2	20.2	16.67	17.32	$9e_{1/2g}$	17.32

[a)] From Ref. [32]. [b)] Our new orbital assignment (see text).
[c)] The peak was not assigned from the PES in Ref. [32].
[d)] The calculated ionization potentials are lower than the experimental result due to the asymptotic error of the DFT method. There is no orbital directly related to peak 8, so we assign peak 8 as the summation of satellite lines.

The momentum–energy density map of $W(CO)_6$ in the region from 5 eV to 25 eV with the electron impact energy of 1200 eV is presented in Fig. 1(a). The qualitative characteristics of each orbital can be immediately obtained from this map, which is very helpful for the orbital assignment. The binding energy spectrum shown in Fig. 1(b) is obtained by summing over all ϕ angles from the momentum–energy density map. With the guide of the PES, eight Gaussian functions are used to fit the experimental binding spectrum. The ionization potentials of the eight peaks determined in the present EMS measurement are 8.6 eV, 13.4 eV, 14.3 eV, 15.0 eV, 15.7 eV, 17.9 eV, 20.2 eV and 23.5 eV, respectively. Peak 1 corresponds to the HOMO $4t_{2g}$ orbital. Overlapped peaks 2–5 correspond to orbitals $11t_{1u}$, $1t_{1g}+2t_{2u}+10t_{1u}$, $3t_{2g}$ and $7e_g+10a_{1g}$, respectively. Peaks 6 and 7 correspond to $9t_{1u}+6e_g$ and $9a_{1g}$, respectively. There is no orbital that is directly related to peak 8, because the next orbital energy is ∼31 eV obtained using the scalar relativistic calculation. Therefore, peak 8 is assigned as the summation of satellite lines resulted from the breakup of the orbital picture.

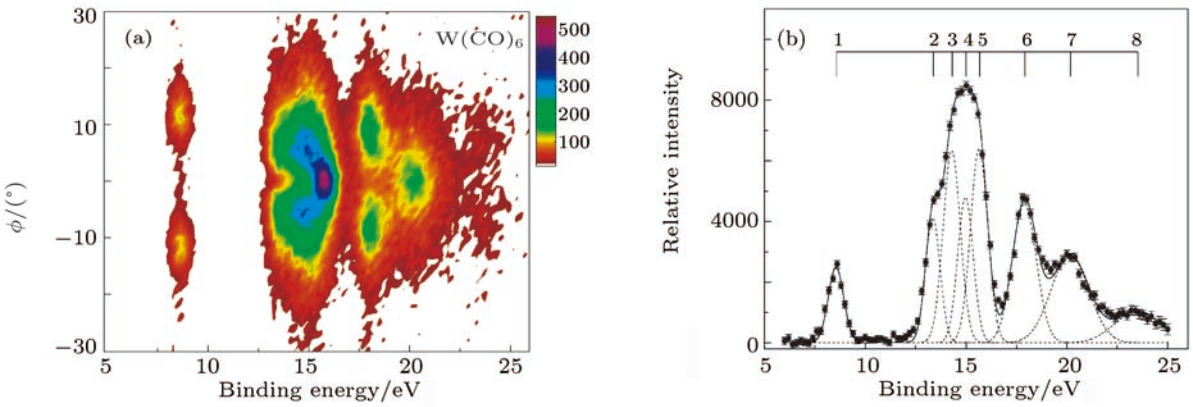


Fig. 1. (a) (colour online) Binding energy–momentum density map of $W(CO)_6$ measured with the impact energy of 1200 eV plus binding energies. (b) Experiment binding energy spectrum summed over all azimuthal angles, the dashed and the solid curves represent individual and summed Gaussian fits, respectively. The positions of individual transitions determined based on the high-resolution PES[29] are shown as bars labeled with numbers 1–8.

3.2. Outer valence orbitals $11t_{1u}$, $1t_{1g}$, $2t_{2u}$, $10t_{1u}$, $3t_{2g}$, $7e_g$, $10a_{1g}$, and their ordering

Peak 2 at 13.4 eV, peak 3 at 14.3 eV, peak 4 at 15.0 eV and peak 5 at 15.7 eV in the binding energy spectrum shown in Fig. 1 are not well separated. They are associated with the ionization from $11t_{1u}$, $1t_{1g}$, $2t_{2u}$, $10t_{1u}$, $3t_{2g}$, $7e_g$ and $10a_{1g}$ orbitals and the energy separations of these orbitals are very small. It is a difficult task to assign these seven orbitals to the four peaks. In addition, the ordering of $10t_{1u}$, $3t_{2g}$ and $7e_g$ has been in dispute. Our calculations suggest the order of

I: $2t_{2u} < 10t_{1u} < 3t_{2g} < 7e_g < 10a_{1g}$,

while the PES work[32] proposed the order of

II: $2t_{2u} < 7e_g < 10t_{1u} < 3t_{2g} < 10a_{1g}$.

The difference between the two sets of orderings lies in the energies of $10t_{1u}$, $3t_{2g}$, and $7e_g$. Although the energy resolution of our spectrometer is not high enough to resolve these orbitals, it has a unique power to identify orbitals and give their ordering. A novel analysis method to study the ordering of orbitals was previously developed and successfully provided a strong support for the correct ordering of $8a'$ and $1a''$ in propene.[44] Based on that method, we cut two energy slices at 14.8–15.2 eV (defined as left) and 15.2–15.6 eV (right) in the map shown in Fig. 1 and define

$$
\begin{aligned}
I(p)_{\text{left}} &= \int_{14.8}^{15.2} \sum_i \rho_i(p) \frac{1}{\sqrt{2\pi}a_i} \\
&\quad \times \exp\left[-\frac{(E-\varepsilon_i)^2}{2a_i^2}\right] \mathrm{d}E, \\
I(p)_{\text{right}} &= \int_{15.2}^{15.6} \sum_i \rho_i(p) \frac{1}{\sqrt{2\pi}a_i} \\
&\quad \times \exp\left[-\frac{(E-\varepsilon_i)^2}{2a_i^2}\right] \mathrm{d}E, \\
\Delta I(p)_{\text{theo}} &= I(p)_{\text{right}} - I(p)_{\text{left}}, \qquad (6)
\end{aligned}
$$

where $\rho_i(p)$ is the theoretical momentum profile (incorporated with the experimental momentum resolution) of the i-th orbital, ε_i is the ionization potential of the i-th orbital obtained from the PES, and a_i is the i-th FWHM divided by $2\sqrt{\ln 4}$. Here, all FWHMs equal to 0.88 eV. The main contribution in this energy region is from orbitals $1t_{1g}$, $2t_{2u}$, $10t_{1u}$, $3t_{2g}$, $7e_g$ and $10a_{1g}$, so other orbitals' contribution is not included in the calculation.

Correspondingly, the experimental data are given by

$$\Delta_{\text{expt}}(p) = \sum_{E=15.2}^{15.6} I_{\text{expt}}(E,p) - \sum_{E=14.8}^{15.2} I_{\text{expt}}(E,p), \quad (7)$$

where $I_{\text{expt}}(E,p)$ is the experimental intensity shown in the map of Fig. 1 and momentum p is related to ϕ by Eq. (1). As illustrated in Fig. 2, it is unanimous that ordering I describes the experimental data better than ordering II, so the correct order should be $2t_{2u} < 10t_{1u} < 3t_{2g} < 7e_g < 10a_{1g}$.

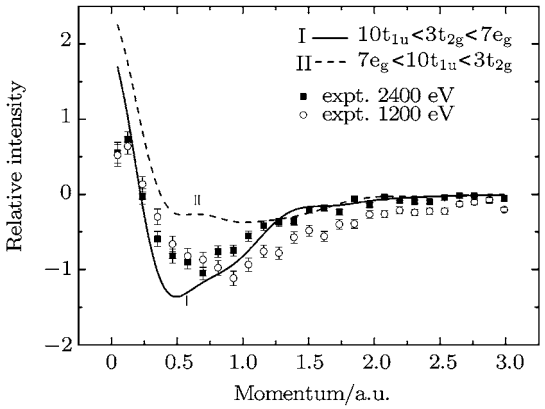


Fig. 2. Measured and calculated differences of the momentum profiles in the energy regions of 14.8–15.2 eV and 15.2–15.6 eV with the impact energies of 1200 eV and 2400 eV plus the binding energies. The calculation using the SR method has been folded with the experimental momentum resolution. See text for details.

Based on our new ordering, peak 2 is tentatively assigned as the HOMO-1 ($11t_{1u}$). As shown in Fig. 3(c), the overall profile of the experimental distribution agrees with the NR, the SR and the SO calculations. However, there is obvious discrepancy in the region of 0.7 a.u. $< p <$ 1.2 a.u.

The experimental momentum distribution of peak 3 shown in Fig. 3(c) is quite different from the momentum profile of HOMO-2 ($1t_{1g}$, Fig. 4(a)), while it is close to the summed theoretical momentum profile of $2t_{2u}$ and $10t_{1u}$. It can be seen that all calculations of $2t_{2u}$+$10t_{1u}$ underestimate the measured intensity in the momentum region of 0.5 a.u. $< p <$ 1.0 a.u..

Figure 3(e) illustrates the experimental momentum distribution of peak 4 in comparison with the theoretical one of $3t_{2g}$. The underestimation of the measured intensity is obvious in the high momentum region.

In the above assignment, one important issue is which peak contains the HOMO-2 ($1t_{1g}$). If we simply added the theoretical momentum profile of $1t_{1g}$

into peak 2 or 3, the obtained intensities would be overestimated too much. The high resolution PES[32] shows that the ionization peak related to $1t_{1g}$ is quite broad, so it may be mixed with peaks 2, 3 and 4. The detailed explanation needs high level calculations of the Frank–Condon factors, the ionization potentials and the pole strengths. However, it is still a challenge to do high level many-body calculations due to the size and the relativistic effects of $W(CO)_6$. So we estimate the mixing coefficients for the best agreement between the theoretical and the experimental momentum distributions. The admixture of $11t_{1u}$+$1t_{1g}\times0.33$ ($0.5\times13u_{3/2u}$ for the SO method), $1t_{1g}\times0.33$ ($0.5\times13u_{3/2u}$ for the SO method)+$2t_{2u}$+$10t_{1u}$ and $1t_{1g}\times0.33$ ($11e_{1/2g}$ for the SO method)+$3t_{2g}$ theoretical momentum profiles reproduces the experimental momentum profiles of peaks 2, 3 and 4, as shown in Figs. 3(b), 3(d), and 3(f).

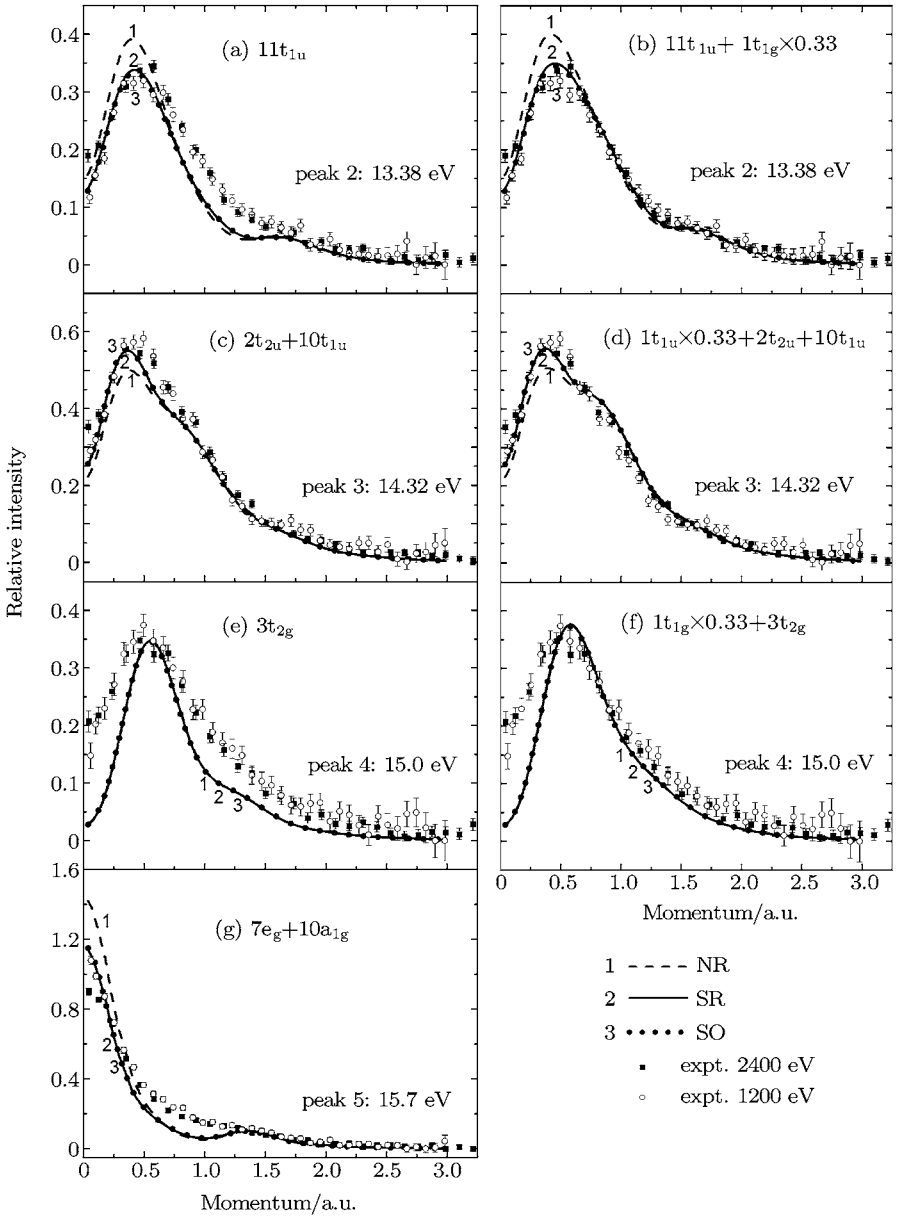


Fig. 3. Measured momentum distributions of peaks 2–5 compared with calculated PWIA momentum distributions of orbitals: (a) peak 2 compared with $11t_{1u}$, (b) peak 2 compared with $11t_{1u}$+$0.33.\times1t_{1g}$, (c) peak 3 compared with $2t_{2u}$+$10t_{1u}$, (d) peak 3 compared with $0.33.\times1t_{1g}$+$2t_{2u}$+$10t_{1u}$, (e) peak 4 compared with $3t_{2g}$, (f) peak 4 compared with $0.33.\times1t_{1g}$+$3t_{2g}$ and (g) peak 5 compared with $7e_g$+$10a_{1g}$. Theoretical momentum profiles are calculated using the NR, the SR, and the SO DFT-B3LYP methods.

It is interesting to note that the sharing of the theoretical intensity of the $1t_{1g}$ orbital among peaks 2, 3 and 4 can largely remove the discrepancy between the experiments and the theories. The exact reason is not clear. One possible explanation is that this orbital has a large broadening in the ionization spectrum.

In Fig. 3(b), it can be seen that the relativistic methods including both the SR and the SO provide excellent predictions for the experimental distribution, while the NR overestimates the measured intensity in the low momentum region of $p < 0.8$ a.u. and somewhat underestimates the measured intensity in the momentum region of 0.8 a.u. $< p <$ 1.5 a.u. Generally, the high momentum region usually corresponds to the small r region in the position space. Therefore, the extensive and dispersive distribution in the experimental momentum profile shown in Fig. 3(b) means that the $11t_{1u}$ or the $1t_{1g}$ orbital shrinks in the position space. The $1t_{1g}$ orbital is almost all from the CO π orbital and is hardly affected by the relativistic effects. As shown in Fig. 4(a), the theoretical momentum profiles for $1t_{1g}$ calculated using the NR and the SR, and the sum of spin–orbital splitting components $11e_{1/2g}$ and $11u_{3/2g}$ calculated using the SO are almost the same. So the shrinkage in the position space mainly happens in the $11t_{1u}$ orbital.

In Fig. 3(d), the summed theoretical momentum distributions calculated using the SR and the SO methods are in excellent agreement with the experimental results, while the NR method underestimates the measured intensity in the low momentum region of $p < 0.6$ a.u. Figure 4(a) demonstrates that there is no difference between the relativistic and the nonrelativistic calculations of $1t_{1g}$. To distinguish the orbital underestimated, $2t_{2u}$ or $10t_{1u}$, the theoretical momentum profiles of both orbitals with the NR, the SR and the SO methods are shown in Fig. 4(b). The theoretical momentum profiles of $2t_{2u}$ generated using three different methods are almost the same, so the relativistic effects do not influence the electron distributions of $2t_{2u}$. It can be seen that the underestimation of the measured intensity in the low momentum region by the NR method primarily occurs for the $10t_{1u}$ orbital. Therefore, the enhanced experimental momentum distribution in the low momentum region means that the $10t_{1u}$ orbital expands in the position space due to the relativistic effects.

Figure 3(e) illustrates the experimental momentum distributions of peak 4 in comparison with the theoretical momentum profiles of $3t_{2g}$. The three different theoretical methods produce almost an identical distribution. It means that the relativistic effects have little influence on the electron distributions of $3t_{2g}$. In Fig. 3(f), the discrepancy in the momentum region of 0.5 a.u. $< p <$ 2 a.u. can be largely removed, if the $1t_{1g}$ orbital is included. However, the experimental intensity in the low momentum region of $p < 0.5$ a.u. is still evidently higher than all theoretical results. A likely reason is the intensity leakage from the next s-type orbital $10a_{1g}$, which has a much higher intensity in the lower momentum region (see Fig. 3(g)).

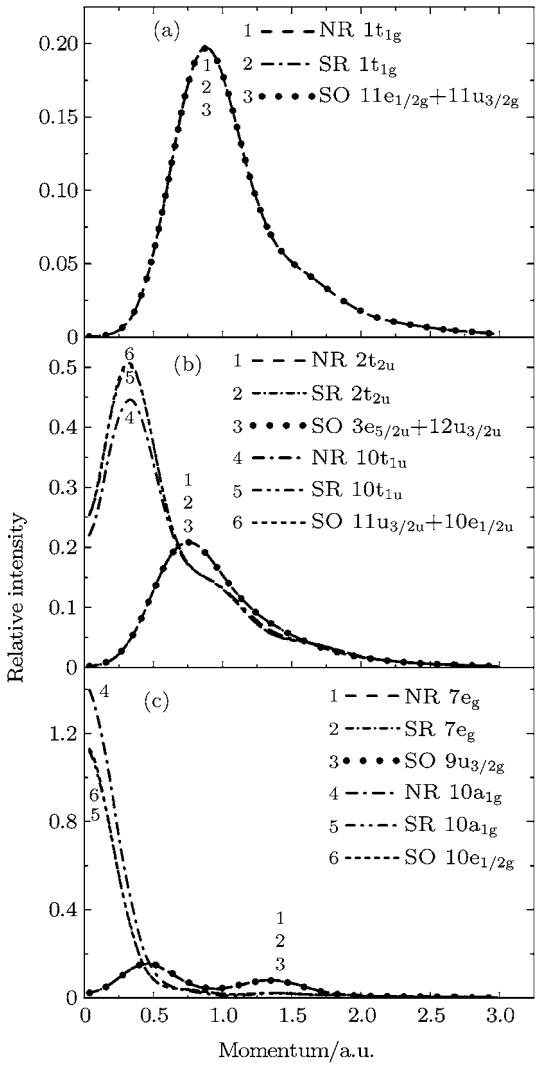


Fig. 4. Theoretical PWIA momentum distributions for (a) $1t_{1g}$, curve 3 denotes the summed $1t_{1g}$ spin–orbital splitting components $11e_{1/2g}$ and $11u_{3/2g}$; (b) $2t_{2u}$ (curves 1, 2 and 3) and $10t_{1u}$ (curve 4, 5 and 6), curve 3 denotes the summed $2t_{2u}$ spin–orbital splitting components $3e_{5/2u}$ and $12u_{3/2u}$, curve 6 denotes the summed $10t_{1u}$ spin–orbital splitting components $11u_{3/2u}$ and $10e_{1/2u}$; (c) $7e_g$ (curves 1, 2 and 3) and $10a_{1g}$ (curves 4, 5 and 6).

Figure 3(g) shows the experimental and the the-

oretical momentum profiles of $7e_g$ and $10a_{1g}$ orbitals. The theoretical momentum distributions obtained using the NR method overestimate the intensity in the low momentum region, while the SR and the SO methods can provide better descriptions for the experimental results, which indicates that the relativistic effects are important for the momentum profiles of $7e_g$ and $10a_{1g}$. Comparing among the theoretical momentum profiles of $7e_g$ and $10a_{1g}$ obtained using the NR, the SR and the SO methods (Fig. 4(c)), we find that the relativistic effects only change the momentum profile of $10a_{1g}$. The lower intensity in the low momentum region indicates that the $10a_{1g}$ orbital shrinks in the position space. In the momentum region of 0.5 a.u. $< p <$ 1.3 a.u., all calculations underestimate the intensity.

The discrepancies between the experimental and theoretical results shown in Figs. 3(f) and 3(g) are probably related to the Gaussian curve fitting and the deconvolution procedures used in the present work, as peaks 3, 4 and 5 in Fig. 1 are not well separated and their Frank–Condon profiles may be asymmetric. It is found that their summed theoretical momentum distribution produces a very good description for the summed experimental result, which partly supports the above explanation.

3.3. Outer valence orbitals $9t_{1u}$, $6e_g$, and $9a_{1g}$

Peak 6 in Fig. 1 corresponds to the ionizations from $9t_{1u}$ and $6e_g$ orbitals, which are too close to be well resolved. In Fig. 5(a), the summed experimental momentum distribution is shown together with the theoretical momentum distributions calculated using the NR, the SR and the SO methods. It can be seen that none of the calculated theoretical momentum profiles is in good agreement with the experimental ones.

Peak 7 in Fig. 1 could be mainly attributed to the ionization from the $9a_{1g}$ orbital. Figure 5(b) shows the experimental momentum distribution in comparison with the theoretical ones. In spite of the poor agreement between the experimental and the theoretical results, the SR and the SO methods produce much higher intensity in the low momentum region than the NR method and make the curves closer to the experimental distributions. The poor agreements between the experiment and the theory shown in Fig. 5 are probably due to the abundant vibrational and satellite structures in the high binding energy region in the BES (Fig. 1), which are also obvious in the PES.[29] These structures make the shapes of peaks 6 and 7 in the BES broad and deviate from the Gaussian one. As a result, the deconvolution procedures using the Gaussian fitting technique can not well separate their individual intensity distributions.

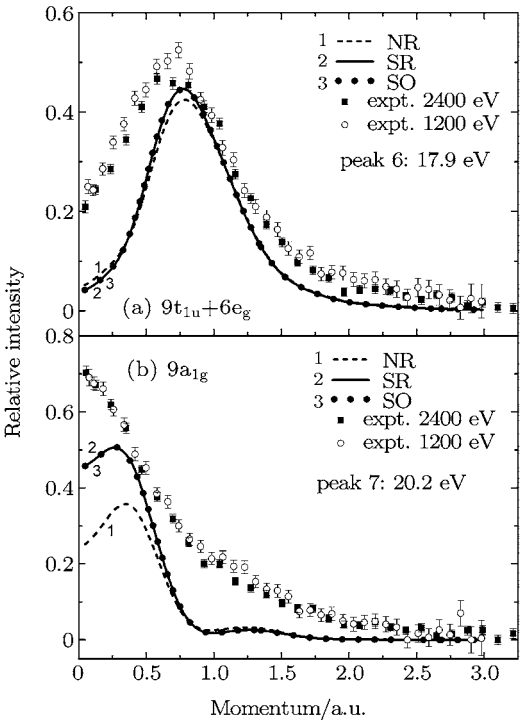


Fig. 5. Experimental and calculated PWIA momentum distributions for (a) $9t_{1u}$+$6e_g$ and (b) $9a_{1g}$ of $W(CO)_6$. The theoretical momentum distributions are calculated using the NR, the SR and the SO DFT-B3LYP methods.

With the Mulliken population analysis for each orbital, it is interesting to note that those orbitals with observable relativistic effects all have contributions from the W 5p or the W 6s electrons, while those orbitals constructed using the electrons from the CO ligands do not show any noticeable relativistic effect.

4. Summary

The experimental momentum profiles for the outer valence shell of $W(CO)_6$ were obtained with the impact energies of 1200 eV and 2400 eV. The theoretical results obtained using the non-relativistic, the scalar relativistic and the spin–orbital relativistic DFT-B3LYP methods were compared with the experimental momentum distributions. In general, the relativistic calculations provided better descriptions for the experiments than the non-relativistic ones, which provided a direct evidence of the influences of the relativistic effects in the outer valence shell of $W(CO)_6$.

The relativistic effects made $11t_{1u}$ and $10a_{1g}$ shrink, $10t_{1u}$ expand in the position space. There were no observable relativistic effect on orbitals $1t_{1g}$, $2t_{2u}$, $3t_{2g}$ and $7e_g$. In addition, the present work proposed the orbital ordering of $10t_{1u} < 3t_{2g} < 7e_g < 10a_{1g}$, which was different from the previous PES work.

References

[1] Dirac P A M 1929 *Proc. R. Soc. London Ser.* A **123** 714

[2] Krause M O, Carlson T A and Woodruff P R 1981 *Phys. Rev.* A **24** 1374

[3] Carlson T A, Fahlman A, Krause M O, Keller P R, Taylor J W, Whitley T and Grimm F A 1984 *J. Chem. Phys.* **80** 3521

[4] Cook J P D, Mitroy J and Weigold E 1984 *Phys. Rev. Lett.* **52** 1116

[5] Cook J P D, Mccarthy I E, Mitroy J and Weigold E 1986 *Phys. Rev.* A **33** 211

[6] Pyykko P 1988 *Chem. Rev.* **88** 563

[7] Grant I P 2007 *Relativistic Quantum Theory of Atoms and Molecules* (New York: Springer Science)

[8] Pepper M and Bursten B E 1991 *Chem. Rev.* **91** 719

[9] Kutzelnigg W 1997 *Chem. Phys.* **225** 203

[10] Liu W J and Dolg M 1998 *Phys. Rev.* A **57** 1721

[11] Liu W J, Dolg M and Li L M 1998 *J. Chem. Phys.* **108** 2886

[12] Velde G T, Bickelhaupt F M, Baerends E J, Guerra C F, van Gisbergen S J A, Snijders J G and Ziegler T 2001 *J. Comput. Chem.* **22** 931

[13] Liu K, Ning C G, Shi L L, Miao Y R and Deng J K 2011 *Acta Phys. Sin.* **60** 023402 (in Chinese)

[14] Liu W J, Wang F and Li L M 2003 *J. Theor. Comput. Chem.* **2** 257

[15] Li J, Bursten B E, Liang B Y and Andrews L 2002 *Science* **295** 2242

[16] Huang W, Pal R, Wang L M, Zeng X C and Wang L S 2010 *J. Chem. Phys.* **132** 054305

[17] Huttula S M, Heinasmaki S, Fritzsche S, Aksela H, Kukk E, Huttula M and Aksela S 2006 *J. Electron. Spectrosc. Relat. Phenom.* **150** 35

[18] Mccarthy I E and Weigold E 1991 *Rep. Prog. Phys.* **54** 789

[19] Coplan M A, Moore J H and Doering J P 1994 *Rev. Mod. Phys.* **66** 985

[20] Weigold E and McCarthy I E 1999 *Electron Momentum Spectroscopy* (New York: Kluwer Academic Plenum Publishers)

[21] Su G L, Ren X G, Zhang S F, Ning C G, Zhou H, Li B, Huang F, Li G Q and Deng J K 2005 *Acta Phys. Sin.* **54** 4108

[22] Li G Q, Deng J K, Li B, Ren X G, Ning C G, Zhang S F and Su G L 2005 *Acta Phys. Sin.* **54** 4669 (in Chinese)

[23] Zhang S F, Ning C G, Huang Y R, Liu K and Deng J K 2009 *Acta Phys. Sin.* **58** 2382 (in Chinese)

[24] Frost L, Mitroy J and Weigold E 1986 *J. Phys.* B: *At. Mol. Opt. Phys.* **19** 4063

[25] Bonfert J, Graf H and Nakel W 1991 *J. Phys.* B: *At. Mol. Opt. Phys.* **24** 1423

[26] Ren X G, Ning C G, Deng J K, Su G L, Zhang S F and Huang Y R 2006 *Phys. Rev.* A **73** 042714

[27] Li Z J, Chen X J, Shan X, Xue X X, Liu T and Xu K Z 2008 *Chem. Phys. Lett.* **457** 45

[28] Liu K, Ning C G and Deng J K 2009 *Phys. Rev.* A **80** 022716

[29] Cotton F A and Wilkinson G 1988 *Advanced Inorganic Chemistry* (New York: Wiley Interscience)

[30] Rolke J, Zheng Y, Brion C E, Chakravorty S J, Davidson E R and McCarthy I E 1997 *Chem. Phys.* **215** 191

[31] Liu K, Ning C G, Luo Z H, Shi L L and Deng J K 2010 *Chem. Phys. Lett.* **497** 229

[32] Higginso. Br, Lloyd D R, Burrough P, Gibson D M and Orchard A F 1973 *J. Chem. Soc. Faraday Trans.* **69** 1659

[33] Duffy P, Chong D P, Casida M E and Salahub D R 1994 *Phys. Rev.* A **50** 4707

[34] Ren X G, Ning C G, Deng J K, Zhang S F, Su G L, Huang F and Li G Q 2005 *Rev. Sci. Instrum.* **76** 063103

[35] Ning C G, Zhang S F, Deng J K, Liu K, Huang Y R and Luo Z H 2008 *Chin. Phys.* B **17** 1729

[36] Guerra C F, Snijders J G, te Velde G and Baerends E J 1998 *Theoretical Chemistry Accounts* **99** 391

[37] ADF 2008 (Amsterdam, The Netherlands: SCM)

[38] Vanlenthe E, Baerends E J and Snijders J G 1994 *J. Chem. Phys.* **101** 9783

[39] Lee C, White D, Suits B H, Bancel P A and Heiney P A 1988 *Phys. Rev.* B **37** 9053

[40] Ehlers A W and Frenking G 1993 *J. Chem. Soc. Chem. Commun.* **22** 1709

[41] Pyykko P 1983 *Chem. Phys.* **74** 1

[42] Visscher L 1996 *Chem. Phys. Lett.* **253** 20

[43] Ning C G, Hajgato B, Huang Y R, Zhang S F, Liu K, Luo Z H, Knippenberg S, Deng J K and Deleuze M S 2008 *Chem. Phys.* **343** 19

[44] Ning C G, Ren X G, Deng J K, Zhang S F, Su G L, Huang F and Li G Q 2005 *J. Chem. Phys.* **122** 224302